JOURNAL OF CATALYSIS 52, 116–132 (1978)

The Oxidative Dehydrogenation of Ethane over Catalysts Containing Mixed Oxides of Molybdenum and Vanadium

E. M. THORSTEINSON,* T. P. WILSON,* F. G. YOUNG,[1,*] AND P. H. KASAI†

* *Union Carbide Technical Center, South Charleston, West Virginia 25303, and*
† *Union Carbide Technical Center, Tarrytown, New York 10591*

Received July 13, 1977; revised November 8, 1977

Mixed oxide catalysts, containing molybdenum and vanadium (MoV) together with another transition metal oxide (Ti, Cr, Mn, Fe, Co, Ni, Nb, Ta, or Ce), are active as low as 200°C for the oxydehydrogenation of ethane to ethylene. A material composed of oxides of composition $Mo_{0.61}V_{0.31}Nb_{0.08}$ appears to be optimum for the reaction. The better MoV catalysts are characterized by a broad X-ray diffraction band near 4.0 Å. The presence of niobium stabilizes the catalyst structure against oxidation and reduction and permits a very strongly oxidized or reduced catalyst to be returned more readily to its original state. The oxydehydrogenation of ethane may involve formation of a surface ethoxide intermediate, since ethanol gives a mixture of both ethane and ethylene with the catalyst in the absence of oxygen. At superatmospheric pressures, acetic acid appears as a product of the subsequent oxidation of ethylene. The kinetics of the process are described. The reaction rates to acetic acid and carbon oxides were found to be dependent on the ethylene concentration but independent of ethane. The catalysts are the basis of a very efficient process for the production of ethylene and acetic acid from ethane. Higher hydrocarbons are nearly completely burned.

INTRODUCTION

The catalytic oxidative dehydrogenation of hydrocarbons has become of major industrial importance only in the last decade (*1*). Highly selective processes for the production of butadiene (*2*), isoprene (*2, 3*), and acrolein (*4*) from mono-olefins have been developed. Oxidative dehydrogenation of paraffin hydrocarbons has not been so successful (*5*). The selectivity to olefins is generally poor because of the low reactivity of the paraffin as compared to the olefin product. The reaction is most successful with paraffins above C-3. Numerous processes for the production of butenes have been described (*6*). Ethane is more refractory than butane, and its catalytic conversion to ethylene has generally proved inefficient. An exception is when a halogen or halogen compound is added to the feed. Then ethylene can be produced efficiently (*7*), but not economically due to the expense attendant upon loss and recovery of the halogen material and due to the severe corrosion of equipment encountered.

We now report an efficient oxidative dehydrogenation of ethane, not requiring halogen, and utilizing catalysts that are so active that significant conversion to ethylene is obtained at a temperature of 200°C.

[1] To whom communications should be addressed.

0021-9517/78/0521-0116$02.00/0

These catalysts consist of a mixture of the oxides of molybdenum and vanadium (MoV) with a variety of third metals (*8*).

Among the most effective catalysts found were an unsupported material having the atomic composition $Mo_{0.73}V_{0.18}Nb_{0.09}$ and a material with the composition $Mo_{0.61}V_{0.31}Nb_{0.08}$ when supported on α-alumina. With the latter material, a selectivity to ethylene of 83% at 25% conversion of ethane has been obtained at 340°C and atmospheric pressure, with a feed of 9.0% ethane, 6% oxygen, and 85% nitrogen. At higher pressures acetic acid appeared as a product of the subsequent oxidation of ethylene initially formed. At 20.4 atm, 325°C, a gas hourly space velocity (GHSV) of 6800, and an ethane/oxygen feed ratio of 19, a combined selectivity to ethylene plus acetic acid of 91.3% was obtained at a molar ratio of (C_2H_4/CH_3COOH) of ~2.5.

EXPERIMENTAL

Catalyst Preparation

Catalysts were prepared in either the neat or supported form. Representative preparations of each are described:

A material comprising oxides of the composition $Mo_{0.61}V_{0.31}Nb_{0.08}$ supported on α-alumina was prepared as follows: ammonium *m*-vanadate (15.9 g, 0.136 g-atom of V) and ammonium paramolybdate (48.1 g, 0.272 g-atom of Mo) were dissolved in 0.5 liter of water while stirring at 85–95°C in a stainless-steel, steam-jacketed evaporating dish. To the resulting solution was added niobium oxalate solution (Kawecki Berylco Chemical Co.) (31.0 g, 0.034 g-atom of Nb). While heating and stirring, 145 g of α-alumina (Norton Co., No. 5218 4 × 8 mesh, irregularly shaped) were added to the mixture. This was followed by evaporation with stirring. Further drying was carried out at a temperature of 120°C for a period of 16 hr. The dried material was then transferred to a wire-screen tray and calcined in an electric furnace for 4 hr at 400°C in ambient air. The amount of material deposited on the support, calculated from its weight increase, was 19.7%. The calculated weight gain for adherence to the support of all of the metal oxides in their highest oxidation states is 28%.

An unsupported material composed of oxides of $Mo_{0.73}V_{0.18}Nb_{0.09}$ was prepared as follows: ammonium *m*-vanadate (40.9 g, 0.350 g-atom of V) was dissolved in 1.0 liter of water while stirring at 85–95°C in a stainless-steel, steam-jacketed evaporating dish. To the resulting solution was added 159.2 g of niobium oxalate solution (0.175 g-atom of Nb) diluted with 100 ml of water and 247 g of ammonium paramolybdate (1.399 g-atom of Mo) dissolved in 800 ml of water. This mixture was heated and dried by evaporation with stirring. Further drying was carried out at a temperature of 120°C for a period of 16 hr. The dried material was broken into 4 × 8-mesh pieces, transferred to a wire-screen tray, and calcined in an electric furnace for 4 hr at 400°C in ambient air.

During these preparations the niobium oxalate was hydrolyzed, and the vanadium (V) was partially reduced by the released oxalic acid, giving blue solutions (*9*). The subsequent chemistry is doubtless very complex, involving the formation of oligomeric anionic species in the acid solutions (*10*).

A number of factors affected the resultant catalytic activity of the MoVNb materials: (i) Catalyst surface area and activity were found to depend on the digestion time, i.e., the time taken to evaporate the solution to dryness. Materials allowed to digest for relatively long periods of time (ca. 30 min) before drying at 120°C underwent particle growth with loss in surface area. The X-ray diffraction patterns of materials digested for long periods and subsequently dried and calcined at 400°C revealed

narrower reflections, indicating larger crystallites, than the corresponding undigested materials. Infrared spectra, however, showed no discernable differences, and the X-ray fluorescence spectra showed no compositional differences. (ii) Calcination at ca. 400°C was found to be optimum for conversion and efficiency. At 500°C considerable sintering occurred as shown by the lower surface areas, leading to lower ethane conversions. Calcination at 300°C resulted in materials having very low efficiencies. (iii) Calcination in air provided the most efficient materials. By contrast, calcining in nitrogen provided materials of lower efficiencies, probably due to reduction by residual ammonia. Neat materials, when dried as small (8 × 12 mesh) pieces gave a more efficient catalyst after calcination than the same material when dried in a large mass and subsequently broken into 8 × 12 mesh. This may be a result of excessive reduction occurring in the larger mass during drying.

Catalyst Characterization

X-ray diffraction (xrd) patterns were determined using plaques of the compressed powdered oxides in a Philips instrument equipped with wide-angle goniometer and using Cu$K\alpha$ radiation. The x-ray photoelectron spectra (xps) were determined on a Hewlett–Packard instrument.

Thermogravimetric analysis was performed using a Cahn electrobalance equipped with a glass vacuum enclosure and having "hang-down tubes" enclosing the sample pan. The sample was heated in a vertical split-tube furnace at a preset rate, while passing nitrogen or air over the sample.

Differential thermal analysis was performed in a Model 900 Dupont instrument equipped with 1200°C high-temperature cell and platinum sample and reference crucibles.

Catalyst Testing and Evaluation

Initial catalyst screening of a variety of metal oxides and metal oxide combinations was done in a pulse microreactor described elsewhere (*8*). In these tests, 2-ml samples of feed gas containing 6.5% oxygen, 8.0% ethane, by volume in nitrogen were injected into a stream of 60 ml/min of helium gas which was passing continually through the catalyst and the close-coupled gas chromatograph. Catalysts were screened for activity by following the composition of the produced pulses as the temperature was increased from 180 to 450°C. Analysis of the product mixture was carried out on a 305 × 0.32-cm stainless-steel column packed with Poropak R. Following sample injection the column was heated at a rate of 10°C/min starting at 30°C. Carbon monoxide was not separated from the air and so was not detected. This lead to exaggeration of the catalyst selectivity when carbon monoxide was a product.

Tubular reactor. Oxides of MoVNb were tested under continuous flow conditions in a tubular reactor at 1 atm total pressure with a feed gas composition of 9.0% C_2H_6, 6.0% O_2, 85% N_2, and a GHSV of 340 hr^{-1}. Catalyst activity was determined at various temperatures. The reactor consisted of a straight 1.27-cm-i.d. stainless-steel tube heated by means of a molten salt bath of ca. 30.5-cm depth. A 0.32-cm-o.d. thermocouple sleeve ran the length of the center of the reactor tube and catalyst bed. The catalyst temperature profile was obtained by sliding the thermocouple in the sleeve. Catalyst, ca. 26 ml, was placed in the tube so that the top of the catalyst bed was ca. 10 cm below the surface of the heat transfer salt. The catalyst bed was 12.7–14.0 cm in length. The zone above the catalyst bed was filled with glass beads to serve as a preheater. The gaseous effluent from the reactor was passed through a condenser and trap at 0°C. Gas and liquid

TABLE 1

Activity and Selectivity of Molybdenum Catalysts

Mixed oxide compositions	Temperature (°C) for initial activity, T_0	Selectivity (%) to C_2H_4 at T_0	Temperature (°C) for 10% conversion, T_{10}	Selectivity (%) to C_2H_4 at T_{10}
$Mo_{0.73}V_{0.18}Nb_{0.09}$	215	100	286	100
$Mo_{0.70}V_{0.17}Ti_{0.09}Mn_{0.04}$	215	100	295	100
$Mo_{0.69}V_{0.17}Ta_{0.06}Fe_{0.03}Si_{0.06}$	220	100	289	100
$Mo_{0.73}V_{0.18}Nb_{0.045}Mn_{0.045}$	243	100	300	100
$Mo_{0.63}V_{0.16}W_{0.06}Mn_{0.16}$	<255	100	295	100
$Mo_{0.70}V_{0.17}Ti_{0.06}Nb_{0.3}Mn_{0.04}$	260	84	400	80
$Mo_{0.70}V_{0.17}Nb_{0.09}Cu_{0.045}$	260	95	330	78
$Mo_{0.70}V_{0.17}Ta_{0.09}Mn_{0.045}$	309	85	385	63
$Mo_{0.70}V_{0.17}Ta_{0.09}Fe_{0.045}$	310	100	418	97
$Mo_{0.5}Mn_{0.5}$	320	100	550–600	35
$Mo_{0.63}Nb_{0.16}W_{0.06}Mn_{0.16}$	328	~100	400	10
$Mo_{0.76}V_{0.19}Fe_{0.05}$	370	100	435	87
$Mo_{0.75}W_{0.25}$	388	100	650	78
$Mo_{0.8}Ti_{0.2}$	390	100	600	65
$Mo_{0.73}Nb_{0.18}W_{0.09}$	~400	—	524	67
$Mo_{1.0}$	418	100	500	88
$Mo_{0.92}V_{0.08}$	444	~100	562	59
$Mo_{0.67}Bi_{0.05}Ti_{0.05}Mn_{0.11}Si_{0.11}$	460	100	505	100
$Mo_{0.75}W_{0.16}Pb_{0.9}$	474	>80	588	72
$Mo_{0.8}V_{0.2}$	500	100	540	100
$Mo_{0.67}V_{0.17}Mn_{0.17}$	502	100	505	100
$Mo_{0.8}Nb_{0.2}$	516	100	634	74

products obtained were analyzed as described below.

Continuous stirred tank reactor (CSTR). The reactor used in the superatmospheric pressure study was a bottom-agitated "Magnedrive" autoclave with a centrally positioned catalyst basket and a side product effluent line (Autoclave Engineers) (*11*). A variable-speed, magnetically driven fan continuously recirculated the reaction mixture through the catalyst bed. The catalyst consisted of 131 g (150 ml) of neat, mixed oxides of the composition $Mo_{0.77}V_{0.19}Nb_{0.04}$ in the form of irregular pieces of 0.64-cm average diameter. Two thermocouples measured the inlet and outlet gas temperatures. The ethane–CO_x mixtures were combined with oxygen before being introduced into the reactor. Liquids, when fed, were pumped into the reactor through the same feed line after the gases were mixed. Condensable liquid products were collected in a series of cold traps at 0 and −78°C.

Analyses

The reactor inlet and outlet gases were analyzed for O_2, N_2, and CO on a 305 × 0.32-cm column of 5A Linde molecular sieves (14/30 mesh) at 95°C, and for (O_2, N_2, CO together), CO_2, ethylene, ethane, and H_2O on a 427 × 0.32-cm column of Poropak Q (80/100 mesh) at 95°C. The liquid product was analyzed for H_2O, ethanol, acetaldehyde, acetic acid, and other components by mass spectrometry. Only traces of acetylene (<1 ppm) were detected in the exit gas using a MoVNb catalyst at 329°C, 1 atm, with a feed of 90% C_2H_6, 10% O_2.

RESULTS

Table 1 gives the results of testing various oxide compositions for activity in

the conversion of ethane to ethylene. The materials are ranked according to the temperature, T_0, at which oxydehydrogenation activity first appeared, and the selectivity, S_0, at this temperature. The selectivity at 10% ethane conversion, S_{10}, is also given at the temperature, T_{10}, required for this.

The results in Table 1 show that the most active oxydehydrogenation catalysts are oxides of molybdenum, vanadium, and another metal niobium, titanium, tantalum, or combinations of them. Two-component molybdenum–vanadium compositions are much less active, but still very efficient catalysts. Less active catalysts result where tungsten replaces vanadium or molybdenum. Addition of iron or copper promotes increased burning and lower ethylene selectivity.

On the basis of these results, further work was directed to molybdenum–vanadium compositions and those containing a third component, especially niobium, because of that element's outstanding ability to increase catalyst activity.

Tubular reactor test data for various α-alumina-supported molybdenum and vanadium oxide (MoV) compositions, with a third-component metal oxide, are given in Table 2. Again the most active and selective were found to be the niobium-containing compositions. Figure 1 is a composition diagram for the three-component MoVNb oxide system showing ethane conversion contours at a 1-atm reaction pressure in the tubular reactor for supported catalysts containing ca. 15–20% oxides of MoVNb. A diagram of ethylene yield contours is identical to Fig. 1, with the highest yield (30%) occurring at the same optimum composition. Under these conditions the optimum compositional area is located within a small molybdenum-rich region, $Mo_{0.61-0.65}V_{0.31-0.27}Nb_{0.08}$. The compositional limits were found to be somewhat broader for the neat (unsupported) materials, i.e., $Mo_{0.61-0.77}V_{0.31-0.19}Nb_{0.08-0.04}$.

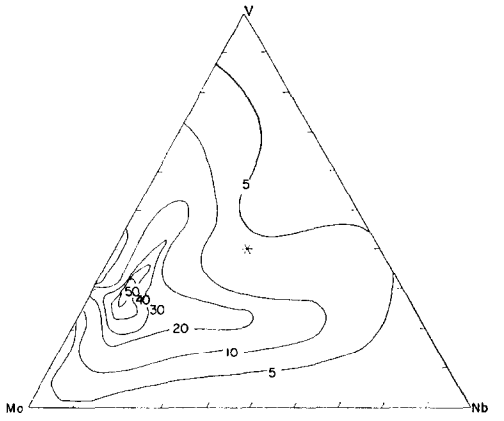

FIG. 1. MoVNb composition diagram showing ethane conversion contours at 400°C. Area within the small closed loop is of highest activity.

TABLE 2

Activities of Selected Compositions Containing Oxides of Molybdenum, Vanadium, and a Third Metal[a]

Composition	Percentage of oxides on support	Conversion (efficiency) at 400°C (%)
$Mo_{0.61}V_{0.31}Nb_{0.08}$	19.7	50 (38)
$Mo_{0.73}V_{0.18}Sb_{0.09}$	13.8	23 (75)
$Mo_{0.57}V_{0.29}Ta_{0.14}$	28.4	18 (77)
$Mo_{0.62}V_{0.30}Ta_{0.08}$	23.4	25 (69)
$Mo_{0.73}V_{0.18}Ti_{0.09}$	30.4	15 (55)
$Mo_{0.30}V_{0.08}Si_{0.62}$	Neat	14 (51)
$Mo_{0.57}V_{0.29}Sb_{0.14}$	23.0	11 (44)
$Mo_{0.64}V_{0.32}Fe_{0.04}$	27.0	9 (45)
$Mo_{0.62}V_{0.30}W_{0.08}$	26.0	7 (61)
$Mo_{0.62}V_{0.30}Sn_{0.08}$	23.1	7 (52)
$Mo_{0.61}V_{0.31}As_{0.08}$	28.4	Trace

[a] Tubular reactor (see Experimental section).

Results of ethane oxydehydrogenation for two-component MoV compositions made in various ways are given in Table 3. None of these was as selective at equivalent ethane conversions as the niobium-containing compositions. Materials with the general composition, $Mo_{0.56}V_{0.28}Nb_{0.08}X_{0.08}$, where X is a first-row transition metal were also tested in an attempt to obtain increased catalytic activity and/or efficiency over that of the unmodified material. The results (Table 4) showed all of the mate-

TABLE 3

Activities of Two-Component MoV Catalysts[a]

Catalyst composition	Percentage of oxides on support	Conversion (efficiency) at 400°C (%)
$Mo_{0.50}V_{0.50}$[b]	22.9	13 (33)
$Mo_{0.49}V_{0.51}$[b]	25.8	16 (23)
$Mo_{0.70}V_{0.30}$[b]	18.5	22 (47)
$Mo_{0.67}V_{0.33}$[c]	22.1	9 (45)
$Mo_{0.49}V_{0.51}$[d]	25.8	3 (50)
$Mo_{0.67}V_{0.33}$[e]	25.9	9 (43) @370°C
$Mo_{0.67}V_{0.33}$[b]	25.9	7 (47)
$Mo_{0.70}V_{0.30}$[b]	27.0	10 (37)
$Mo_{0.80}V_{0.20}$[c]	Neat	2 (87) @300°C
$Mo_{0.80}V_{0.20}$[c]	Neat	2 (63)
$Mo_{0.40}V_{0.60}$[e]	Neat	19 (18)

[a] Tubular reactor (see Experimental section).
[b] Normal preparation for supported catalyst.
[c] Oxalic acid equivalent to V added.
[d] Calcined at 500°C.
[e] Made from MoO_3 and V_2O_5 in HCl.

rials were less active and some less efficient than the unmodified version. Compositions supported on silica gel were quite active but inefficient.

Reaction Studies at Superatmospheric Pressures

Experiments were carried out in a CSTR using the unsupported catalyst $Mo_{0.73}V_{0.18}Nb_{0.09}$ at 20.4 atm, 275–325°C, 6800 GHSV, and reactor inlet conditions 95% C_2H_6, 5% O_2. A fraction of this catalyst was analyzed as: Mo, 55.59 wt%; V, 7.44 wt%, by atomic absorption, and as Nb, 2.68 wt%, by flame emission spectrometry, corresponding to a molar composition of $Mo_{0.77}V_{0.19}Nb_{0.04}$. At temperatures above ca. 340°C under these conditions and in the absence of catalyst, the unselective homogeneous oxidation of ethane occurred. This was quenched somewhat by the presence of catalyst. Below 340°C, combined efficiencies to ethylene and acetic acid above 90% were obtained (Table 5). With the above conditions and catalyst at 325°C, the rate of production of ethylene was 9.55 g-mol liter^{-1} hr^{-1} and of acetic acid 3.74 g-mol liter^{-1} hr^{-1}. The amount of ethylene relative to acetic acid produced increased with decreasing conversion. The product solutions contained ca. 40–45 wt% acetic acid in water. The highest impurity concentration was ethanol at less than 0.1 wt%.

Oxidation Kinetics

Empirical expressions were derived for the rate of ethane oxidation and ethylene, acetic acid, and carbon oxides formation as functions of temperature (275 to 325°C) and the partial pressures of ethane (4–20 atm), ethylene (0.1–1.0 atm), oxygen (0.03–0.36 atm), carbon dioxide (0.003–0.38 atm), carbon monoxide (0.0001–0.70 atm), and water (0.14–0.83 atm). Sixteen experiments comprising a 2^{7-3} fractional factorial designed set were carried out. To this data set were added three centerpoint replicates and experiments with added acetic acid (up to 0.18 atm) and water (up to 2.0 atm), and at high oxygen concentrations (up to 0.84 atm). The rates of production of ethylene, acetic acid, carbon monoxide and carbon dioxide are represented by the expressions given below. Only integral and half-integral powers of product and reactant pressures and poisoning terms were per-

TABLE 4

Activity Data for Catalysts, $Mo_{0.56}V_{0.28}Nb_{0.08}X_{0.08}$[a]

X	Percentage of oxides on supports	Conversion (efficiency) at 300°C (%)
—	19.7	12 (91)
Mn	25.4	4 (97)
Co	26.3	6 (94)
Ni	26.4	5 (93)
Ce	28.0	9 (84)
Fe	23.0	8 (82)
Cu	25.1	6 (79)
Cr	24.2	2 (87)

[a] Tubular reactor (see Experimental section).

mitted. Langmuir–Hinshelwood poisoning terms were incorporated into the expressions for the C_2H_4 and CO rates. No temperature dependence was included in the poisoning terms. Rates are given in gram-moles (product) per gram (catalyst) per hour. Partial pressures are in atmospheres, and temperature is in degrees Kelvin.

$$r_{C_2H_6} = \frac{-1.730 \times 10^3 e^{-5625/T} P_{C_2H_6} P_{O_2}}{(1 + 2.286 P_{C_2H_4} + 14.63 P_{O_2})^2}; \qquad [X_{mult} = 0.82]^2$$

$$r_{HOAC} = \frac{3.29 \times 10^4 e^{-5632/T} P_{C_2H_4} P_{O_2} P_{H_2O}}{(1 + 1.843 P_{C_2H_4} + 4.215 P_{O_2} + 1.465 P_{H_2O})^3}; \qquad [X_{mult} = 0.78]$$

$$r_{CO} = \frac{1.755 \times 10^{11} e^{-15270/T} P_{C_2H_4} P_{O_2}}{(1 + 0.3119 P_{C_2H_6} + 6.83 P_{C_2H_4})^2}; \qquad [X_{mult} = 0.80]$$

$$r_{CO_2} = \frac{2.396 \times 10^5 e^{-9318/T} P_{C_2H_4} P_{O_2}^{\frac{1}{2}}}{(1 + 3.787 P_{C_2H_4})^2}; \qquad [X_{mult} = 0.51]$$

$$r_{C_2H_4} = -r_{C_2H_6} - r_{HOAC} - r_{CO}^{\frac{1}{2}} - r_{CO_2}^{\frac{1}{2}}.$$

For ethane consumption and acetic acid and carbon monoxide production, about 80% of the variability in the experimental rate data is accounted for by the empirical rate expressions. The fit is not as good for carbon dioxide; that equation accounts for only 51% of the variability in the data.

Ethylene production from ethane appears strongly inhibited by ethylene. The acetic acid and carbon oxide rates depend on ethylene and oxygen partial pressures, suggesting that they are formed by a reaction sequence in which ethane is first dehydrogenated to ethylene and ethylene is then oxidized further. The acetic acid rate is also dependent on the partial pressure of water. There is no evidence for oxidation of CO to CO_2 over this catalyst, and the evidence for further oxidation of acetic acid is ambiguous.

When ethanol was passed over the fresh catalyst, $Mo_{0.73}V_{0.18}Nb_{0.09}$, at 350°C and a 1-atm total pressure without added oxygen the products were: ethane, 0.33 mol; ethylene, 0.40 mol; acetic acid, 0.1 mol; acetaldehyde, 0.15 mol; carbon dioxide, 0.03 mol; carbon monoxide, 0.01 mol; and water, 0.68 mol/mol of ethanol fed. Since ethane is a prominent product of this reaction, it is concluded that the reduction of ethanol and the oxydehydrogenation of ethane involves a common intermediate. This may be surface ethoxide (*vide infra*).

Higher Hydrocarbons

Passage of propane, 94%, with oxygen, 6%, over the composition $Mo_{0.67}V_{0.25}Nb_{0.08}$ at 300°C resulted in consumption of all of the oxygen, giving acetic acid, acetalde-

[2] The variable X_{mult} is defined as follows:

$$X_{mult} = 1 - \frac{\sum_i [r_i(obs) - r_i(calc)]^2}{\sum_i [r_i(obs) - r_i(avg)]^2},$$

where r_i(calc) is the rate calculated from a model derived from a least-squares fit to the observed rates, r_i(obs). The sum in the denominator represents the total variability present in the experimental data; i.e., the sum of squares of the deviations of the observed rates about a mean, r_i(avg). The sum in the numerator represents the residual sum of squares of the deviation of the observed rates from the rates calculated from the model. X_{mult} represents the fraction of the original variability in the data accounted for by the model. A perfect fit would be implied by an X_{mult} of 1.

TABLE 5

Ethane Oxidation at 20.4 atm over the Catalyst $Mo_{0.77}V_{0.19}Nb_{0.04}$[a]

Temperature (°C)	Conversion (%)	Efficiency to C_2H_4 (%)	Efficiency to CH_3COOH (%)	Total efficiency (%)	$\frac{C_2H_4}{CH_3COOH}$
275	1.9	69.7	19.1	88.8	3.7
300	3.7	70.0	23.5	93.5	3.0
325	5.2	65.5	25.8	91.3	2.5

[a] Continuous stirred tank reactor (see Experimental section).

hyde, and carbon oxides as products. *n*-Butene was likewise extensively burned at 250–300°C. This hyperactivity is presumably due to the presence of a labile allylic hydrogen in the olefin, giving a center for oxidative attack.

Sulfur Poisoning

Passage of hydrogen sulfide with ethane and oxygen over the composition $Mo_{0.73}V_{0.18}Nb_{0.09}$ at 300°C resulted in consumption of all the oxygen and oxidation of all of the hydrogen sulfide. Subsequently, after removal of the hydrogen sulfide from the feed, the catalyst activity was completely recovered and the efficiency of oxydehydrogenation of ethane returned quickly to its previous high value.

Catalyst Characterization

X-ray. Table 6 gives X-ray diffraction and specific activity data for MoV compositions made according to directions in (*12*) and (13*a*). The phase chemistry in the molybdenum–vanadium oxide system has been described (*12*, *13a*). In the presence of excess molybdenum oxide, reduced, vanadium-rich phases appear. Between 18.5 and 33 atom% vanadium, the two phases, $Mo_4V_6O_{25}$ (I) and $Mo_6V_9O_{40}$ (II),

TABLE 6

Materials Tested for Oxydehydrogenation of Ethane to Ethylene[a]

Bulk composition	Relative intensity at			Conversion (efficiency) at 350°C (%)	Surface area (BET) (m^2g^{-1})	Specific activity at 350°C (percentage conversion/m^2)
	4.00 Å	4.06 Å	4.12 Å			
$Mo_{0.73}V_{0.18}Nb_{0.09}$[b]	Strong	Medium (shoulder)	Weak	58.0 (65)	11.7	0.169
$Mo_{0.75}V_{0.25}$[c]	Strong	Medium	Weak	2.6 (90)	4.9	0.133
$Mo_{0.40}V_{0.60}$[d]	Weak (shoulder)	Strong	Strong	8.0 (50)	7.1	0.059
$Mo_{0.40}V_{0.60}$[d]	Weak	Weak (shoulder)	Strong (shoulder)	12.6 (24.5)	10.1	0.053
$Mo_{0.75}V_{0.25}$[c]	Very weak	Weak	Very weak	0.6 (86)	3.2	0.010

[a] Tubular reactor (see Experimental section).
[b] Normal preparation for supported catalyst.
[c] Composition made from $NH_4Mo_6O_{24} + V_2O_5$ in HCl; precipitated with EtOH.
[d] Made from MoO_3 and V_2O_5 in HCl.

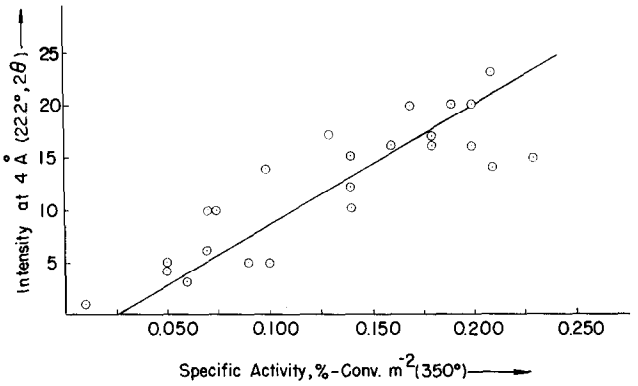

FIG. 2. Intensity of X-ray diffraction (xrd) reflection at 4.00 Å vs specific activity (percentage conversion m^{-2}) for oxides of composition $Mo_{0.80-0.61}V_{0.20-0.31}Nb_{0.0-0.08}$.

are the principal constituents of the mixed oxide, the remaining fraction being orthorhombic and/or hexagonal MoO_3 phases. This is precisely the optimum compositional range for selective ethane oxidation to ethylene and acetic acid; i.e., $Mo_{0.61-0.77}V_{0.31-0.19}Nb_{0.08-0.04}$. I and II are thought to be the principal constituents of commercial catalysts used for the oxidation of benzene to maleic acid and are interconvertible by oxidation–reduction (*12*, *13a*). The compound $Mo_4V_6O_{25}$ (Phase I) has its strongest reflection at 4.06 Å, and $Mo_6V_9O_{40}$ (Phase II) has its strongest reflection at 4.12 Å. V_2MoO_8 also has its strongest reflection at 4.12 Å. Table 6 shows that MoV oxide compositions giving strong (but diffuse) reflections at 4.00 Å have the highest specific activities in ethane oxydehydrogenation. Materials having strong X-ray lines only at 4.06 or 4.12 Å have much lower activity. Furthermore, the specific activity of 24 MoV-containing catalysts was found to be roughly proportional to the intensity of their 4.00-Å X-ray reflection (Fig. 2). The conclusion is that (the surfaces of) Phases I and/or II are not the most active in the composition, but that activity is somehow associated with a material giving the 4.00-Å reflection.

Nevertheless, Phases I and II represent the thermodynamically controlled equilibrium condition of the MoV oxide system containing 18.5 to 33 atom% vanadium. Since the xrd patterns show only the 4.00-Å reflection and reflections that can be ascribed to orthorhombic and/or hexagonal MoO_3, it is reasonable to assume that the 4.00-Å reflection arises from vanadium-containing material. Furthermore, it is probably a precursor (albeit a defective one) of Phases I and II and is vanadium-rich.

Figure 3, patterns A–D, shows the X-ray powder patterns of the Mo–V–Nb composition obtained after successive reduction and oxidation treatment. The X-ray powder patterns of the Mo–V system obtained after the identical series of treatments are shown in Figure 4, patterns A–D. Figures 5 and 6 show, respectively, the sequential changes observed in the X-ray powder patterns of the Mo–V–Nb and the Mo–V systems when subjected successively to oxidation and reduction treatments.

Inspections of these figures reveal the following: (i) The diffused peak at 4.00 Å attributed to a meta-stable, layered defect phase appears much more conspicuously in the powder pattern of the Mo–V–Nb sample (Fig. 3, pattern A) than that of the Mo–V sample (Fig. 4, pattern A). (ii) The "defect phase" of the Mo–V–Nb system is much more resistant to the medial reduction as well as the medial oxidation treatments. (iii) Under reducing conditions (C_2H_6 at

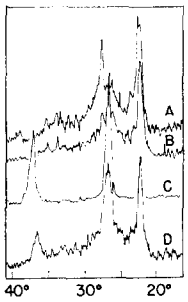

FIG. 3. The xrd patterns of the MoVNb composition during the reduction–oxidation cycle: (A) initial catalyst; (B) same after reduction for 1 hr at 400°C in ethane, 0.75 atm; (C) same after 17 hr; (D) same after reoxidation for 1 hr at 300°C in oxygen, 0.75 atm.

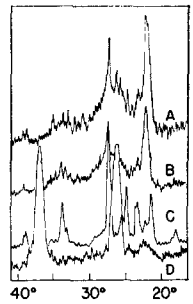

FIG. 5. The xrd patterns of the MoVNb composition during the oxidation reduction cycle: (A) initial catalyst; (B) same after oxidation for 1 hr at 400°C in oxygen, 0.75 atm; (C) same after 17 hr; (D) same after reduction for 17 hr at 400°C in ethane, 0.75 atm.

400°C), a well-crystallized $Mo(V)O_2$ phase is eventually formed in both the Mo–V–Nb and Mo–V systems (Figs. 3 and 4). (iv) Under oxidizing conditions (O_2 at 400°C), the eventual formation of MoO_3 and V_2MoO_8 was noted for both systems (Figs. 5 and 6). (v) All of these crystal modification processes are readily reversible as shown by pattern D in each sequence. Of particular interest is *the regeneration of the 4.00-Å defect phase when the extensively reduced Mo–V–Nb system was subjected to a mild oxidation treatment* (Fig. 3, pattern D).

We conclude that a Mo–V oxide composition, with or without Nb, constitutes an extremely efficient intermediary for the oxidation process. The presence of Nb stabilizes the 4.0-Å defect phase, which may provide a geometry conducive to a highly selective oxidation. Niobium also affects the crystallinity as shown, in Fig. 7, by the xrd patterns of two materials made in identical ways, but with and without Nb. The material lacking the niobium was made with an equivalent amount of oxalic acid, so that the reducing conditions of the preparation were the same for each. The material, $Mo_{0.80}V_{0.20}$, gave the pattern with the narrower reflections; i.e., was more crystalline. Of particular note is the fact that the sharp reflection at 4.07 Å for $Mo_{0.80}V_{0.20}$ was broadened to include a rather diffuse but strong reflection at 4.00 Å, in the niobium-containing material. The conclusion is that the presence of niobium slows the rate of formation of one or both of Phases I and II during catalyst preparation.

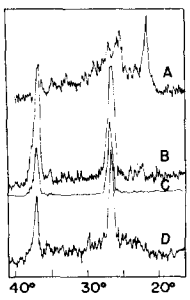

FIG. 4. The xrd patterns of the MoV composition during the reduction–oxidation cycle. (A)–(D) as in Fig. 3.

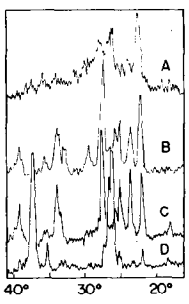

FIG. 6. The xrd patterns of the MoV composition during the oxidation–reduction cycle. (A)–(D) as in Fig. 5.

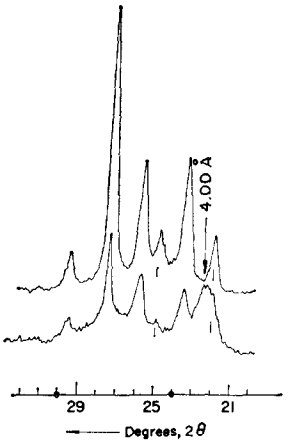

FIG. 7. The xrd patterns showing effect of niobium on crystallinity, $Mo_{0.80}V_{0.20}$ (upper) vs $Mo_{0.73}V_{0.18}Nb_{0.09}$ (lower).

ESR

The ESR spectra of MoVNb and MoV materials (Fig. 8) showed a single, essentially isotropic signal at g = 1.97 which is close to that expected from $V^{4+}(3d^1)$, $Nb^{4+}(4d^1)$ or $Mo^{5+}(4d^1)$. The unpaired electron density was estimated to be 10^{18} spins g^{-1}. The presence of this type of signal suggests that the materials, as prepared, are slightly reduced relative to the metals in their highest oxidation states.

Most of the Mo isotopes possess nonmagnetic nuclei. The rather large line widths of the signals are therefore attributed to broadening by the magnetic nuclei ^{51}V (natural abundance $\cong 100\%$, $I = \frac{7}{2}$, $\mu = 6.1435\beta_N$). The lack of well-resolved

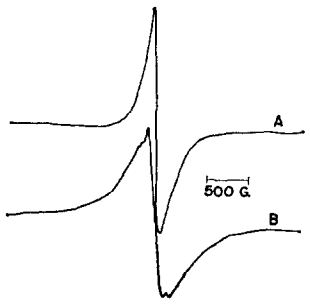

FIG. 8. ESR spectra of initial catalyst: (A) MoVNb; (B) MoV.

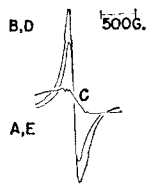

FIG. 9. ESR spectra of MoVNb catalyst after sequential reduction and oxidation: (A) initial catalyst; (B) ethane 1 hr at 120°C; (C) ethane 2 hr at 300°C; (D) oxygen 1 hr at 400°C; (E) oxygen 17 hr at 400°C.

hyperfine structure and the isotropy of the signal suggest delocalization of the unpaired electrons, however. The signal observed with the MoVNb system is narrower (ΔHpp = 150 G) than that of MoV (ΔHpp = 300 G), indicating a more efficient delocalization process in the former.

Figure 9, patterns A–E, shows the sequential change of the ESR signal exhibited by a MoVNb sample when it was subjected to a reduction–oxidation cycle. The signal, after being dramatically reduced by reduction, was completely restored to its initial level by oxidation. A similar sequential change was observed with the MoV system. The reduction of the signal after the medial reduction treatment is attributed to a disproportionation reaction of the type; $2Mo^{5+} \rightarrow Mo^{6+} + Mo^{4+}$, or to the reduction to Mo^{4+} and lower valent species. No ESR signal was observed from $Mo^{4+}(4d^2)$ ions. The reversible sequence shown in Fig. 9 thus can be written as follows:

$$2\,Mo^{6+} \underset{O_2/400°C}{\overset{C_2H_6/120°C}{\rightleftharpoons}} 2\,Mo^{5+} \underset{O_2/300°C}{\overset{C_2H_6/300°C}{\rightleftharpoons}} Mo^{6+} + Mo^{4+}$$

When subjected to an extensive reducing treatment (C_2H_6, 0.75 atm, 400°C, 17 hr), the electrical conductivities of both the MoVNb and the MoV composition increased to such an extent that ESR measurements were no longer possible. The increased electrical conductivity indicates removal of a significant amount of oxygen

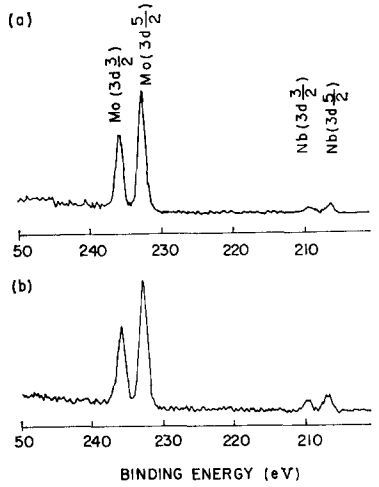

FIG. 10. The X-ray photoelectron spectra (xps) spectra of Mo ($3d_{\frac{3}{2}}$, $3d_{\frac{5}{2}}$) and Nb ($3d_{\frac{3}{2}}$, $3d_{\frac{5}{2}}$) region: (a) initial MoVNb catalyst; (b) extensively reduced MoVNb catalyst.

from the material. This is supported by the TGA, below. The X-ray powder pattern showed that both types of systems are converted to a MoO_2-type material when subjected to such a treatment.

X-ray Photoelectron Spectra (xps)

Compared in Fig. 10 are the xps spectra of the Mo ($3d_{\frac{3}{2}}$, $3d_{\frac{5}{2}}$) and Nb ($3d_{\frac{3}{2}}$, $3d_{\frac{5}{2}}$) region obtained from the initial and the extensively reduced (C_2H_6, 0.75 atm, 400°C, 17 hr) MoVNb samples. Two conclusions can be drawn immediately: (i) The intensity of the Nb peaks relative to that of Mo increases significantly as the sample is reduced, indicating the migration of Nb toward the surface during the reduction. (ii) The valence state of the "surface" Mo (as revealed by the binding energy) is +6 in both the initial and the reduced samples (*13b*). The latter conclusion is particularly significant as the X-ray powder pattern of the reduced sample (Fig. 3, pattern C) showed that its bulk composition is MoO_2. The oxidation of the surface layer by the ambient atmosphere must be responsible for this difference.

To examine the surface oxidation process, fresh samples of the extensively reduced MoV and MoVNb compositions were prepared in a vacuum manifold and placed in sealed tubes. The sealed samples were then broken and transferred into the spectrometer with minimum exposure to the ambient atmosphere. The xps spectra of the reduced Mo and the reduced MoV system thus obtained, and those obtained after having these samples exposed to the ambient atmosphere for 7 and 48 hr, respectively, are shown in Fig. 11. The spectral sequence obtained from the reduced MoVNb sample was identical to that of the MoV system. It is thus clearly demonstrated that the surface of pure MoO_2 is fairly stable and that the presence of vanadium strongly facilitates the reoxidation of Mo^{4+} to Mo^{6+} at the surface. The +5 oxidation states are apparently not very stable for Mo. This is consistent with the disproportionation reaction, $2\,Mo^{5+} \rightarrow Mo^{4+} + Mo^{6+}$, proposed to account for the decrease of the ESR signal due to Mo^{5+} (Fig. 9, pattern C).

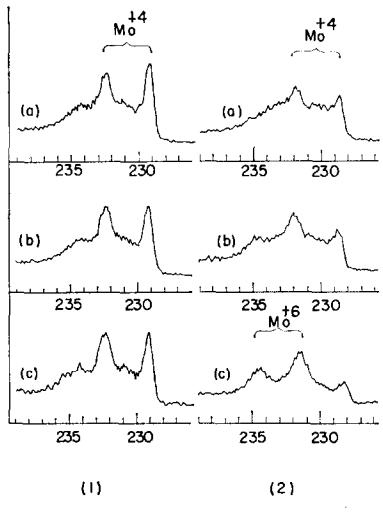

FIG. 11. The xp spectra, Mo ($3d_{\frac{3}{2}}$, $3d_{\frac{5}{2}}$), of (1) MoO_2 and (2) $Mo(V)O_2$. (a) Initial catalyst, (b) after 7 hr of exposure to air, (c) after 48 hr of exposure.

TABLE 7

Comparison of the Bulk and the Surface Compositions of MoVNb Catalysts

Bulk composition			Bulk composition		Surface composition[a]	
Mo	V	Nb	[V]/[Mo]	[Nb]/[Mo]	[V]/[Mo]	[Nb]/[Mo]
0.38	0.57	0.05	1.50	0.13	1.44	0.14
0.62	0.31	0.08	0.50	0.13	0.56	0.13
0.73	0.18	0.09	0.25	0.13	0.25	0.13
0.84	0.11	0.05	0.13	0.06	0.26	0.11
0.84	0.05	0.11	0.06	0.13	0.11	0.18

[a] Determined from the area of the xps signals. The uncertainties in the area determinations are ± 10%.

Surface Profile

Several fresh MoVNb catalysts of differing bulk compositions were examined by xps. The areas of the Mo ($3d_{\frac{3}{2}}$, $3d_{\frac{5}{2}}$), V ($2p_{\frac{1}{2}}$, $2p_{\frac{3}{2}}$), and Nb ($3d_{\frac{3}{2}}$, $3d_{\frac{5}{2}}$) doublets were measured for each sample and attempts were made to determine the surface profile, [V]/[Mo] and [Nb]/[Mo].

The intensity of an xps peak depends on the cross section for the X-ray photoionization of the particular electron involved and the probability of escape of the electron from the material without interaction. Wagner (*14*) has measured the relative intensities of the strongest xps peaks of many elements in the periodic table. Included in his tables are the Ti ($2p_{\frac{3}{2}}$) and Mo ($3d_{\frac{5}{2}}$) peaks. More recently Scofield (*15*) completed theoretical cross section calculations for photoionization of the individual subshells for all the elements within $Z = 1$ to 101. From the theoretically calculated cross sections and the empirically determined sensitivities of the Ti ($2p_{\frac{3}{2}}$) and Mo ($3d_{\frac{5}{2}}$) peaks, the relative sensitivities of the V ($2p_{\frac{1}{2}}$, $2p_{\frac{3}{2}}$), Nb ($3d_{\frac{3}{2}}$, $3d_{\frac{5}{2}}$), and Mo ($3d_{\frac{3}{2}}$, $3d_{\frac{5}{2}}$) doublets can be calculated, the results being 0.59, 0.87, and 1.00, respectively.

Table 7 lists the MoVNb catalysts examined, their bulk compositions, and the surface compositions as determined from the relative intensities of the xps signals corrected by the relative sensitivities above. The table reveals clearly that when the catalyst contains comparable amounts of Group V (V and Nb) and Group VI (Mo) elements, the surface profile [V]/[Mo] and [Nb]/[Mo], is very close to that of the bulk. On the other hand, when molybdenum is present in excess of the concentrations, the Group V elements in the surface layer are much higher than those in the bulk. In compound semiconductors, impurity cations of lower valence than the cations of the host lattice are frequently observed to diffuse toward the surface or to aggregate there.

TGA

Figure 12 shows the weight loss of $Mo_{0.61}V_{0.31}Nb_{0.08}$ in ethane at 375°C and the regain of weight in oxygen. The weight loss is divided into three regions: (i) a very rapid loss amounting to about 1% of its weight; (ii) a slower loss, roughly linear in time, up to 6–7% of its weight; and (iii) a slowing and final steady state in ethane at about 9% weight loss. On reoxidation in air, the weight is regained extremely rapidly at first, two-thirds of it within a few minutes, followed by a much slower gain continuing over many hours. If the reduction is limited to the first very rapid stage, reoxidation is extremely rapid and complete.

Figure 13 illustrates the dependence of the redox cycle upon temperature, which was increased at a rate of 8°C/min in these

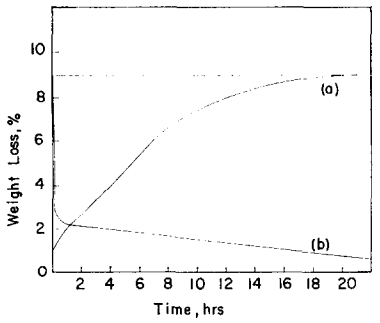

FIG. 12. Thermogravimetry of $Mo_{0.61}V_{0.31}Nb_{0.08}$ at 375°C (a) in ethane and (b) in oxygen.

experiments. Reduction in ethane starts at about 250°C and increases more rapidly at higher temperatures. If the extent of catalyst reduction corresponds to less than 3% weight loss, reoxidation by oxygen is complete, and the redox cycle can be repeated. The conclusion is that lattice oxygen is very labile, and oxygen deep within the bulk can participate in reduction and reoxidation at the surface.

DTA

Differential thermal curves for several oxide compositions containing molybdenum are shown schematically in Fig. 14. The endothermic feature at 795°C present in (d), $Mo_{0.8}Ti_{0.2}$, is due to the melting of MoO_3 (*16*). Uncombined MoO_3 is apparently not present in the other compositions, nor is uncombined vanadium pentoxide (mp, 800°C). The transition at 760°C appearing in (b), $Mo_{0.8}V_{0.2}$, and as a shoulder in (a), $Mo_{0.73}V_{0.18}Nb_{0.09}$, may be due to the phase change of $Mo_{18}O_{52}$(tricl.) to Mo_9O_{26}(mon.) (*16*), or to the decomposition of a θ-phase, $Mo_{1-x}V_xO_{2.80}$, where $0.06 \leqslant x \leqslant 0.11$ given in Ref. (*17*) as occurring at 765°C. The peak at 815°C in (f) may indicate the presence of orthorhombic Mo_4O_{11} (*16*).

Endothermic peaks at 610 and 740°C are common to MoVNb materials, (a), (b), and (f). Their assignment is uncertain, especially since a shoulder at 610°C also occurs in $MnMoO_4$, (e).

DISCUSSION

The principal question to be addressed is, "Why is the MoVNb oxide composition such an active catalyst for the oxydehydrogenation of ethane?" Its great activity is evident by comparison with chromia gel. With chromia gel, conversion of ethane to ethylene is only 0.5% at 400°C (*18*), while with the oxide catalyst, $Mo_{0.73}V_{0.18}Nb_{0.09}$, reaction starts at 215°C and reaches 10% ethane conversion at 286°C. The conversion over chromia gel is an equilibrium-limited reaction, and the oxydehydrogenation is not. However, since the two reactions were carried out in reactors of similar geometry at similar space velocities, the comparison is valid.

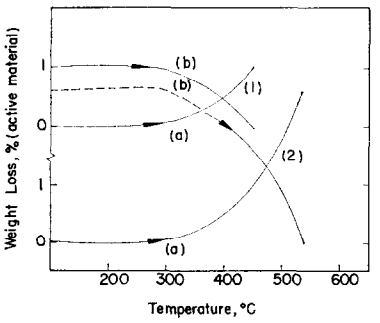

FIG. 13. Thermogravimetry of $Mo_{0.61}V_{0.31}Nb_{0.08}$ as a function of temperature. (1) First cycle and (2) second cycle (a) in ethane and (b) in oxygen.

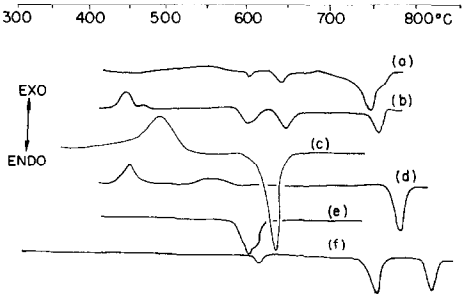

FIG. 14. DTA of mixed molybdenum oxide compositions: (a) $Mo_{0.73}V_{0.18}Nb_{0.09}$; (b) $Mo_{0.8}V_{0.2}$; (c) $Mo_{0.63}V_{0.16}W_{0.06}Mn_{0.16}$; (d) $Mo_{0.08}Ti_{0.2}$; (e) $MnMo_4$; (f) $Mo_{0.5}V_{0.125}Nb_{0.375}$.

Molybdenum oxide itself has only a slight activity in the reaction (Table 1). The addition of vanadium does not increase the activity of MoO_3 very much, but additions of both vanadium and niobium result in a very active (and highly selective) catalyst. The freshly made three-component catalyst is highly colored and is reduced somewhat below the fully oxidized state. At this stage, this catalyst exhibits an ESR signal, which may be attributed to Mo^{5+}. If V^{4+} contributed greatly, some hyperfine structure should be visible, but it is not. The ESR signal is not due to Nb^{4+}, since Nb-free catalysts still show the color and signal.

The ESR signal disappears on treatment with ethane at mild conditions, forming equivalent amounts of Mo^{6+} and Mo^{4+}. Ethanol reacts with the fresh catalyst in the absence of oxygen to give both ethylene and ethane. Ethane reacts with the fresh catalyst, either in the absence or presence of oxygen, to give ethylene. If added oxygen is present, the production of ethylene becomes catalytic. These features suggest the cyclic catalysis mechanism (Scheme I).

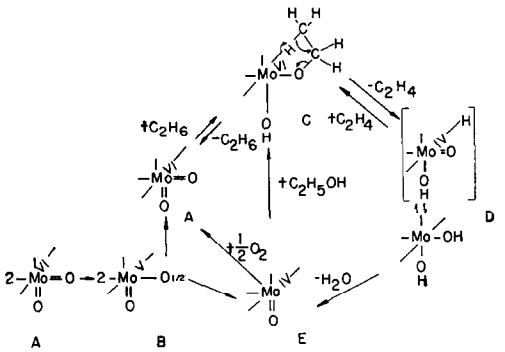

SCHEME I

In this mechanism two adjacent Mo^{6+} atoms at the catalyst surface participate. Each molybdenum carries at least two oxo ligands (A). With the loss of oxygen thermally by roasting or by the partial reduction with ammonia or oxalic acid in the preparation step, the Mo^{6+} atoms are reduced to a Mo^{5+} species (B). This explains the color and presence of an ESR signal in a fresh (unused) catalyst. The species B can now disproportionate to a pentacoordinate Mo^{4+} species, (E), and to Mo^{6+}, which may be coordinately unsaturated (cus). This happens by gentle treatment of the initial catalyst with ethane, and the ESR signal disappears. In the catalytic oxidation, ethane reacts with an oxo ligand on Mo^{6+} (cus), giving an ethoxy–hydroxy species (C). This is a reasonable expectation since molybdates are known to react with hydrocarbons to give hydroxylated species (*19*).[3]

The ethoxy species (C) is of a configuration such that a hydrogen on the methyl group could be close to an uncoordinated site on molybdenum, thus activating this β-hydrogen. Cotton *et al.* (*20*) have shown a related effect in the compound $[Et_2B(pz)_2]Mo(CO)_2(\eta^3\text{-allyl})$, where the α-hydrogen of the axial ethyl group lies only 2.2 Å from the molybdenum atom, so close indeed that the H–Mo bond must be regarded as a three-center, two-electron bond. This implies activation of the α-hydrogen by the geometrical constraint in the six-membered ring. In C the ring would be five-membered. Due to this activation, transfer of the β-hydrogen to molybdenum occurs with simultaneous release of ethylene. This produces the species D, containing an oxo, hydroxyl, and hydride ligand group attached to the same molybdenum IV atom. This should be unstable, and facile rearrangement to a Mo IV dihydroxy species should occur. Alternately, after activation in C, ethylene could be expelled in a concerted four-center process giving the Mo IV dihydroxy species directly. Loss of water from the dihydroxy

[3] The oxidation of butadiene over titania–molybdena catalysts is attributed to the oxo ligand on Mo^{6+}, developed by oxidation of Mo^{5+} at the surface [Akimoto, M., and Echigoya, E., *J. Catal.* **29**, 191 (1973)]. Such a molybdenum oxo species is indicated here.

species gives the five-coordinate Mo^{4+} species, E, present, to a smaller degree, in the fresh catalyst.

The production of ethane and ethylene from ethanol passed over the fresh catalyst without additional oxygen, can be rationalized by involving this species, E. Dissociative adsorption of ethanol on E, leads to the species C directly. C can either desorb ethane, giving A, or desorb ethylene, giving D. The catalytic oxidation cycle is completed by reoxidation of the Mo IV species E to the molybdenum VI species A.

Vanadium enters into the catalysis in the reoxidation of Mo^{4+} to Mo^{6+}. This is supported by the xps results (Fig. 10) showing a more facile reoxidation of MoO_2 containing vanadium than without it. Niobium also plays a role in the reoxidation process, since in the reduced MoVNb composition (Fig. 4) the defect phase represented by the xrd feature at 4.0 Å is more readily restored by oxidation than it is in the niobium-free material (Fig. 3).

The fact that ethanol reacts with the fresh catalyst to give ethane indicates that the fresh catalyst already contains a reduced cus species. This lends support to the assertion that some reduction occurs in the catalyst preparation, and that some five-coordinate Mo^{4+} is present even before the catalyst sees ethane.

An alternative hypothesis (Scheme II) could involve reaction of ethane with a molybdenum dioxo species (A), forming an hydroxy-alkoxy molybdenum, which then decomposes in a concerted process, giving water, ethylene, and the molybdenum (IV) oxo species (E).

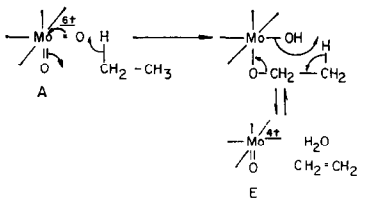

SCHEME II

Scheme I or II accounts for the primary reaction products with ethane and with ethanol, as well as the spectral and oxidation–reduction properties of the molybdenum-containing catalysts. The scheme bears some analogy to that suggested for the molybdenum-containing oxidases and reductases (*21*) in which the reducing property of reductases is attributed to five-coordinate Mo^{4+}, and the oxidizing property of oxidases is assigned to a Mo^{6+} dioxo species.

Kinetics of the process. Under superatmospheric pressure acetic acid becomes a coproduct of the reaction. The empirical rate equation for acetic acid production shows a first-order dependence upon the partial pressure of ethylene and oxygen, but is independent of the ethane partial pressure. Likewise, the expressions for the production of carbon oxides show independence of the ethane partial pressure. This strongly suggests that the primary oxydehydrogenation product of ethane is ethylene and that acetic acid and carbon oxides are formed by its subsequent oxidation. The role of water upon the acetic acid production rate is informative. The somewhat reduced state of the fresh catalyst implies the presence of bare metal sites, which in the presence of water acquire Brönsted acid character. Tin–molybdenum oxide catalysts for the oxidation of propylene to acetone indeed give higher conversion in the presence of water. The reaction apparently involves the protonation of the olefin giving an isopropoxide species (*22*). The oxidation of ethylene to acetic acid may involve an analogous first step, giving an ethoxide species, $MOH + C_2H_4 = MOC_2H_5$. Certainly this oxidation of ethylene to acetic acid is well-known for molybdenum- and vanadium-containing catalysts (*22*).

ACKNOWLEDGMENTS

The authors wish to acknowledge the efforts of C. E. Jett, H. J. Decker, and E. F. Mills in the

preparation and testing of the catalysts, and of Francis V. Kalu for operation of the CSTR in the superatmospheric pressure studies. D. McLeod, Jr. took all of the ESR and xps spectra and a large part of the xrd spectra. His creative interpretation of these is greatly appreciated. M. Habenschuss did many of the kinetic measurements and developed the kinetic equations from them. We also wish to thank F. A. Cotton and A. W. Naumann for several discussions and suggestions. Thanks are due to Union Carbide Corporation for permission to publish this work.

REFERENCES

1. Wolf, C. N., Bergman, R. I., and Sittig, M., *Chem. Week*, May 28, 1966, p. 113.
2. Voge, H. H., Armstrong, W. E., and Ryland, L. B., U. S. Patent 3,110,746, November 12, 1963.
3. Callahan, J. L., Gertisser, B., and Grasselli, R., U. S. Patent 3,260,768, July 12, 1966.
4. Veath, F., Callahan, J. L., Milberger, E. C., and Foreman, R. W., *in* "Actes Congress International Catalyse 2e," Paris 1960, Vol. 2, p. 2647 (1961).
5. Adams, C. R., *in* "Symposium on Catalytic Oxidation of Hydrocarbons," New York, September 7–12, 1969, Vol. 14, No. 4, p. C6.
6. Manning, H. E., U. S. Patent 3,780,126, December 18, 1973; Walker, D. E., U. S. Patent 3,830,868, August 20, 1974.
7. Nager, M., U. S. Patent 3,080,435, March 5, 1963.
8. Young, F. G., and Thorsteinson, E. M., Belgium Patent 846,778, April 1, 1977.
9. Sathyanarayana, D. N., and Patel, C. C., *J. Inorg. Nucl. Chem.* **27**, 297 (1965).
10. Trifiro, F., Forzatti, P., and Villa, P. L., *in* "International Symposium on Scientific Basis for the Preparation of Heterogeneous Catalysts," Brussels, Belgium, October 14–17, 1975.
11. Berty, J. M., Hambrick, J. O., Malone, T. R., and Ullock, D. S., *in* "Symposium on Advances in High-Pressure Technology," 64th National Meeting of the American Institute of Chemical Engineers, New Orleans, La., March 16–20, 1969.
12. Ponsolle, L., Wrobel, G., and Germain, J. E., *J. Microsc.* **7**, 949 (1968).
13. (a) Munch, R. H., and Pierron, E. D., *J. Catal.* **3**, 406 (1964); (b) For the binding energies of Mo($3d_{\frac{5}{2}}$) and Mo($3d_{\frac{3}{2}}$) at various oxidation states, see Swartz, W. E., and Hercules, D. M., *Anal. Chem.* **43**, 1774 (1971).
14. Wagner, C. D., *Anal. Chem.* **44**, 1050 (1972).
15. Scofield, J. H., Lawrence Livermore Laboratory, Report No. UCRL-51326, January 1973.
16. Ekstrom, T., and Nygren, M., *Acta Chem. Scand.* **26**, 1830 (1972).
17. Ekstrom, T., and Nygren, M., *Acta Chem. Scand.* **26**, 1844.
18. Frey, F. E., and Huppke, W. F., *Ind. Eng. Chem.* **25**, 54 (1933).
19. Schuit, G. C. A., *in* "First International Conference on Chemistry and Uses of Molybdenum," Reading, England, September 17–21, 1973.
20. Cotton, F. A., LaCour, T., and Stanislowski, A. G., *J. Amer. Chem. Soc.* **96**, 754 (1974).
21. Wentworth, R. A. D., *Coord. Chem. Rev.* **18**, 1 (1976).
22. Takita, Y., Ozaki, A., and Moro-Oka, Y., *J. Catal.* **27**, 185 (1972).
23. Rottig, W., French Patent 1,395,378, April 9, 1965; DelVesco, A., and Gurdjan, V., Belgium Patent 687,720, March 16, 1967.